High Resolution Structures of the 4–4–20 Fab-Fluorescein Complex in Two Solvent Systems: Effects of Solvent on Structure and Antigen-Binding Affinity

James N. Herron,* Alan H. Terry,* Steven Johnston,* Xiao-min He,‡ Luke W. Guddat,§ Edward W. Voss, Jr.,¶ and Allen B. Edmundson§

*Department of Pharmaceutics and Pharmaceutical Chemistry, University of Utah, Salt Lake City, Utah 84112; ‡Marshall Space Flight Center, NASA, Huntsville, Alabama; §Harrington Cancer Center, Amarillo, Texas; and ¶Department of Microbiology, University of Illinois, Urbana, Illinois 61801 USA

ABSTRACT Three-dimensional structures were determined for three crystal forms of the antigen binding fragment (Fab) of anti-fluorescein antibody 4–4–20 in complex with fluorescein. These included 1) a triclinic ($P1$) form crystallized in 47% (v/v) 2-methyl-2,4-pentanediol (MPD); 2) a triclinic ($P1$) form crystallized in 16% (w/v) poly(ethylene glycol), molecular weight 3350 (PEG); and 3) a monoclinic ($P2_1$) form crystallized in 16% PEG. Solvent molecules were added to the three models and the structures were refined to their diffraction limits (1.75-Å, 1.78-Å, and 2.49-Å resolution for the MPD, triclinic PEG, and monoclinic PEG forms, respectively). Comparisons of these structures were interesting because 4–4–20 exhibited a lower antigen-binding affinity in 47% MPD ($K_a = 1.3 \times 10^8\ M^{-1}$) than in either 16% PEG ($K_a = 2.9 \times 10^9\ M^{-1}$) or phosphate-buffered saline ($K_a = 1.8 \times 10^{10}\ M^{-1}$). Even though the solution behavior of the antibody was significantly different in MPD and PEG, the crystal structures were remarkably similar. In all three structures, the fluorescein-combining site was an aromatic slot formed by tyrosines L32, H96, and H97 and tryptophans L96 and H33. In addition, several active site constituents formed an electrostatic network with the ligand. These included a salt link between arginine L34 and one of fluorescein's enolate oxygen atoms, a hydrogen bond between histidine L27d and the second enolic group, a hydrogen bond between tyrosine L32 and the phenylcarboxylate group, and two medium range (~5 Å) electrostatic interactions with lysine L50 and arginine H52. The only major difference between the triclinic MPD and PEG structures was the degree of hydration of the antigen-combining site. Three water molecules participated in the above electrostatic network in the MPD structure, while eight were involved in the PEG structure. Based on this observation, we believe that 4–4–20 exhibits a lower affinity in MPD due to the depletion of the hydration shell of the antigen-combining site.

INTRODUCTION

Antibodies are archetypal of a number of different proteins in the immunoglobulin supergene family, which makes them excellent model systems for studying problems of molecular recognition in the immune system. In particular, by studying antigen-antibody interactions at the molecular level, we hope to comprehend how structural elements translate into the affinity and specificity of antigen-combining sites. Such mechanistic models should facilitate the engineering of antibodies and related proteins for applications in clinical diagnostics, medical imaging, and targeted drug delivery.

Several three-dimensional structures of antigen-antibody complexes have been reported in the last decade. These include: 1) complexes with proteins such as lysozyme, neuraminadase, histidine-containing protein (HPr), and human immunodeficiency virus type 1 (HIV-1) reverse transcriptase (Amit et al., 1986; Colman et al., 1987; Sheriff et al., 1987; Colman et al., 1989; Padlan et al., 1989; Davies et al., 1990; Jacobo-Molina et al., 1993; Prasad et al., 1993); 2) complexes with synthetic peptides derived from myohemerythrin, influenza hemagglutinin, and HIV-1 envelope glycoprotein gp120 (Stura et al., 1989; Stanfield et al., 1990; Rini et al., 1992, 1993; Ghiara et al., 1994); 3) complexes with haptens such as fluorescein, 2-phenyloxazolone, phosphocholine, progesterone, and cyclosporin A (Padlan et al., 1985; Herron et al., 1989; Alzari et al., 1990; Altschuh et al., 1992; Arevalo et al., 1993; Vix et al., 1993); and 4) a complex with a deoxynucleotide (Herron et al., 1991). Several structures have been compared in recent review articles (Davies et al., 1990; Mian et al., 1991; Wilson et al., 1991; Wilson and Stanfield, 1993). There appear to be several components to specific binding, including the topology of the antigen-combining site, the amount of solvent-accessible surface area

Received for publication 1 July 1993 and in final form 21 September 1994.

Address reprint requests to James N. Herron, Department of Pharmaceutics and Pharmaceutical Chemistry, 421 Wakara Way, Ste. 316, Salt Lake City, UT 84108. Tel.: 801-581-7216; Fax: 801-581-7848; E-mail: herron@bioiris.med.utah.edu.

Abbreviations used: 3-D, three-dimensional; Arg, arginine; C_α, α carbon; C_β, β carbon; CDR, complementarity-determining region; C_H1, first constant domain of the immunoglobulin heavy chain; C_L, constant domain of the immunoglobulin light chain; DTE, dithioerythritol; Fab, antigen-binding fragment; F_c, calculated structure factor; F_o, observed amplitude of the structure factor; Gly, glycine; H2, second complementarity-determining region of the immunoglobulin heavy chain; H3, third complementarity-determining region of the immunoglobulin heavy chain; His, histidine; HIV-1, human immunodeficiency virus type I; IgG, immunoglobulin G; L1, first complementarity-determining region of the immunoglobulin light chain; L2, second complementarity-determining region of the immunoglobulin light chain; Lys, lysine; MD, molecular dynamics; MPD, 2-methyl-2,4-pentanediol; PBS, phosphate-buffered saline; PEG, poly(ethylene glycol); rms, root mean square; Ser, serine; Trp, tryptophan; Tyr, tyrosine; V_H, variable domain of the immunoglobulin heavy chain; V_L, variable domain of the immunoglobulin light chain.

0006-3495/94/12/2167/17 $2.00

(including both antigen and antibody) that is buried upon binding, and electrostatic interactions such as hydrogen bonds and salt links. Moreover, recent studies in our group, as well as in Ian Wilson's laboratory, have shown that there is a fourth mechanism (induced fit) that in some cases enables the antibody to change its conformation in order to achieve greater complementarity (Herron et al., 1991; Rini et al., 1992; Arevalo et al., 1993).

Of the above antigen-antibody complexes, the anti-fluorescein 4–4–20 system is the best characterized in solution. Physicochemical information has been obtained for 4–4–20 and related antibodies over the past decade, including antigen-binding affinities under different conditions (Kranz et al., 1982; Herron, 1984; Gibson et al., 1988; Omelyanenko et al., 1993), kinetics (Kranz and Voss, 1981; Kranz et al., 1981, 1982; Herron and Voss, 1983; Herron, 1984), thermodynamics (Herron et al., 1986; Gibson et al., 1988), and amino acid sequences (Reinitz et al., 1988; Bedzyk et al., 1989, 1990a, b; Dombrink-Kurtzman et al., 1989). Furthermore, the three-dimensional structure of the 4–4–20 Fab/fluorescein complex was determined at 2.7-Å resolution by our group in 1989 (Herron et al., 1989). This study indicated that fluorescein binds tightly in an aromatic slot and participates in a network of electrostatic interactions.

In our original studies, crystals were grown in 47% (v/v) MPD and crystallized in a triclinic space group ($P1$). Since high concentrations of diols such as MPD and glycerol are sometimes used to elute antibodies from affinity chromatography columns, we decided to compare the affinity and thermodynamics of the 4–4–20/fluorescein complex in phosphate-buffered saline (PBS) and 47% MPD. We found that the affinity was ~140-fold lower in MPD than in PBS (Gibson et al., 1988). This posed the question of whether the decrease in affinity was due exclusively to solvent effects or if the fundamental structure of the antigen-combining site had changed as well. We were able to crystallize the 4–4–20 Fab/fluorescein complex in PEG (3350 molecular weight), which we thought would be a more "native" crystallizing agent (Gibson et al., 1988). Two crystal forms were obtained in PEG: 1) a triclinic ($P1$) form nearly isomorphous to the MPD form and 2) a monoclinic form ($P2_1$) with one Fab fragment per asymmetric unit. Since the original structure of the 4–4–20 Fab/fluorescein complex was reported, the x-ray analyses have been extended to 1.75-Å resolution for the MPD form, to 1.78-Å resolution for the triclinic PEG form, and to 2.5-Å resolution for the monoclinic PEG form. The structures of the three complexes are compared in detail in this article.

MATERIALS AND METHODS

Crystallographic analysis

The 4–4–20 Fab-fluorescein complex was prepared and crystallized as described by Gibson et al. (1988). Crystals were grown in either 47% (v/v) MPD or 16% (w/v) PEG-3350. Samples crystallized with PEG early in the project were found to have monoclinic space groups and were mostly twinned. Later samples purified under more stringent requirements of light exclusion and temperature control (13 ± 2°C) produced crystals with triclinic space groups and crystal morphology nearly identical with MPD forms. Diffraction data were collected with a Siemens-Nicolet P21 diffractometer equipped with a scintillation detector and helium chamber. Space groups were initially determined using 8° or 10° precession photos, although the lattice parameters used for structure determination were obtained from diffractometer data. In cases where indexing was difficult, 3° precession photos were used to align the crystal and adjust the arcs of the goniometer. Diffraction data were collected using an omega step scan procedure (Wyckoff et al., 1967) and intensities were corrected for background, absorption, and radiation damage as previously described (Edmundson et al., 1972). Four crystals were used to collect the data set for the MPD form. An attempt was made to extend the data to d spacings of 1.5-Å, but the reflections were mostly unobserved beyond 1.75-Å. The PEG triclinic form was particularly resistant to radiation damage, and only one crystal was required for data collection. One crystal was sufficient for the PEG monoclinic form, but the data extended only to 2.5-Å resolution.

Molecular replacement

Molecular replacement techniques (Rossmann and Blow, 1962; Lattman and Love, 1970; Crowther, 1972; Cygler and Anderson, 1988a, b; Fitzgerald, 1988) were used to determine the orientations of the Fabs within the unit cells of the two PEG forms. The 1.75-Å structure of the MPD form was used as a starting model. The fast rotation function (Crowther, 1972) was used to find the rotational orientations of the V_L-V_H pair and the C_L-C_H pair, and then those of individual domains. Next, these orientations were "fine-tuned" using the Lattmann-Love rotation function (Lattman and Love, 1970). The translational orientations of the four domains were determined either with the MERLOT program (Fitzgerald, 1988) or a real space translational searching program (RTMAP) written by one of us (X.M.H.). Finally, the positions of the four domains were refined by constrained-restrained least square refinement with the program CORELS (Herzberg and Sussman, 1983).

Crystallographic refinement and model building

Once the low resolution structures of the PEG crystal forms were determined, crystallographic refinement techniques were used to extend the phases of all three structures to higher resolution. Structures were first refined by simulated annealing with X-PLOR (Brünger et al., 1987) using the standard topology and parameter files (TOPH19x and PARAM19x). The slow cooling (4000 K to 300 K) protocol was used, followed by energy minimization (with x-ray terms included). Electron density maps [F_o-F_c OMIT maps (Bhat and Cohen, 1984), and $2F_o$-F_c maps] were then examined using the molecular graphics program Turbo FRODO (Roussel and Cambillau, 1989). This process was repeated three to five times until each structure stabilized. At this point, the structures were solvated as described in Results and refined again by simulated annealing. In this case, however, a more abbreviated temperature range was used (2000 K to 300 K, after the initial placement of the water molecules; and 1000 K to 300 K, thereafter) along with the force field parameters described by Engh and Huber (1991). Restrained least-squares refinement with PROLSQ (Hendrickson and Konnert, 1981) was used to produce the final structure. Coordinate errors were estimated by two different methods: Luzzati's method for determining the overall rms error of the structure from the variation in R value with resolution (Luzzati, 1952) and Cruickshank's formulae for estimating individual coordinate errors from Fourier methods (Cruickshank, 1949, 1950, 1954; Fujinaga et al., 1985). In the latter case, estimated coordinate errors were computed using a program (SIGMA) written by Steven Sheriff (Bristol-Myers Squibb). This program was modified by two of us (X.M.H. and J.N.H.) for monoclinic and triclinic space groups.

Affinity measurements using fluorescence methodology

Fluorescence methodology and algorithms for determining the affinity of anti-fluorescein antibodies were previously described by one of us (Herron,

1984). Fluorescence measurements were made using a photon-counting spectrofluorometer (model PC-1, ISS, Champaign, IL). Samples were excited with plane polarized light at 485 nm. Emission was measured at 515 nm with the emission polarizer first parallel, and then perpendicular. Emission data were corrected for polarization dependencies in the detection system ("g-factor" correction) and then used to determine fluorescence intensity and steady-state anisotropy values. Fluorescence measurements were taken at several different concentrations of PEG-3350 over a range of 0% to 20% (w/v) and used to compute the antigen-binding affinity (K_a).

RESULTS

Affinity measurements

As mentioned in the Introduction, the antigen-binding affinity of 4–4–20 was lower in the two solvent systems used to crystallize the Fab fragment than in PBS. Although we had previously characterized the affinity of 4–4–20 dissolved in aqueous solutions of MPD (Gibson et al., 1988), similar data had not been obtained for 4–4–20 in PEG solutions. For this reason, the affinity of 4–4–20 was determined in aqueous solutions of PEG-3350, varying from 0% to 20% (w/v). These data are presented in Fig. 1 *B*. Comparable data for the MPD form are shown in *A*. Affinity values are listed in Table 1 for the solvent compositions in the crystallization media. The affinity is 6.2-fold lower (1.1 kcal mol^{-1}) in 16% PEG and 138-fold lower (2.9 kcal mol^{-1}) in 47% MPD than in PBS. Although neither solvent is "physiological," the affinity of the PEG form is much closer to that in a "native" environment than the MPD form.

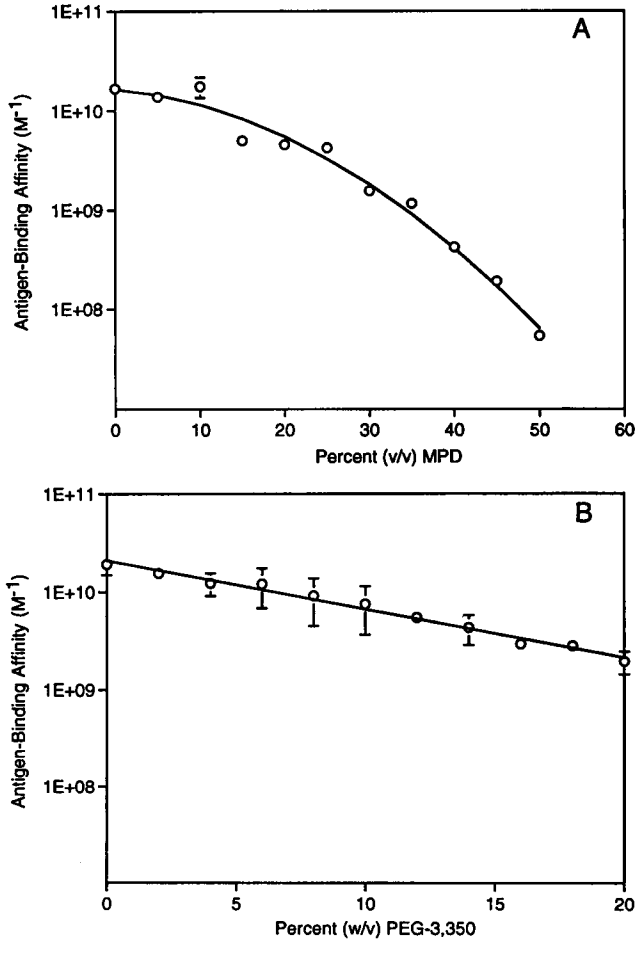

FIGURE 1 Antigen-binding affinity of 4–4–20 in MPD (*A*) and PEG-3350 (*B*). Affinity values were determined by fluorescence quenching assay (Herron, 1984). The 4–4–20 Fab/fluorescein complex was crystallized in 47% MPD and 16% PEG-3350.

X-ray diffraction data

The lattice parameters, resolution limits, and merging statistics are presented in Table 2. The lattice parameters of the two triclinic forms differed by <1% (Table 2); when their data sets were scaled and compared, they exhibited a "goodness of fit" parameter (R_f, see Table 2 for definition) of 0.190 over a resolution range of 1.78 Å to ∞. Together, these observations indicated that the two triclinic forms were nearly isomorphous but probably exhibited subtle differences in their tertiary structures. Another interesting observation was that the *a* and *b* cell dimensions of the triclinic PEG form were very similar in length to the *a* and *c* dimensions of the monoclinic PEG form (Table 2). Furthermore, the β-angle of the monoclinic form (95.2°) was supplementary to the γ-angle of the triclinic form (84.7°). These observations suggested that the orientation of the Fab in the *ab* plane of the triclinic form may be similar to that in the *ac* plane of the monoclinic form. Data sets for the MPD form were merged by scaling common shells (6.5-Å to ∞) for the four crystals. The merging statistics (R_m, see Table 2 for definition) for these crystals ranged from 7% to 9% (Table 2).

Amino acid sequences

The amino acid sequences of the variable domains (V_L and V_H) of 4–4–20 are shown in Fig. 2. They were deduced from nucleotide sequences as described previously (Bedzyk et al., 1989, 1990a). Two different sequence numbering systems were used: 1) a strict sequential numbering system (used in

TABLE 1 Antigen-binding affinity of 4–4–20 in different solvent systems

Solvent	Affinity (M^{-1})	$\Delta\Delta G°_{PBS}$ (kcal mol^{-1})
PBS	$1.8 \pm 0.3 \times 10^{10}$	0.0
PEG	$2.9 \pm 0.4 \times 10^{9}$	1.1
MPD	$1.3 \pm 0.3 \times 10^{8}$	2.9

Antigen-binding affinities were determined by fluorescent quenching assay (Herron, 1984). All measurements were performed at 25°C. Affinities were determined in three different solvent systems: 1) 50 mM sodium phosphate, 100 mM NaCl, pH 6.8 (PBS); 2) 16% (w/v) poly(ethylene glycol) (3350 MW), dissolved in PBS, pH 6.8 (PEG); and 3) 47% (v/v) 2-methyl-2,4-pentanediol, dissolved in PBS, pH 6.8 (MPD). To evaluate the destabilizing effects of the different solvent systems, the difference in standard free energy (for the formation of the 4–4–20/fluorescein complex) was calculated relative to PBS ($\Delta\Delta G°_{PBS}$). Positive values represent destabilizing effects.

TABLE 2 Crystal systems and x-ray diffraction data for 4–4–20

Protein	Space group	*a* (Å)	*b* (Å)	*c* (Å)	α (°)	β (°)	γ (°)	Resolution of data (Å)	Number of crystals
				Crystal systems*					
MPD	*P*1	58.3	43.9	42.5	82.1	87.3	84.6	1.75	4
PEG	*P*1	58.2	44.1	42.9	81.6	86.5	84.7	1.78	1
PEG	$P2_1$	58.6	97.2	44.5	90.0	95.2	90.0	2.49	1

		Crystal no.	Resolution range	Number of reflections	Number observed	Inter-crystal R_m
			Diffraction data‡			
MPD	*P*1	1	2.5-∞	14,451	10,271	
		2	2.1–2.5	9,477	6,983	0.082
		3	1.8–2.1	12,963	5,680	0.089
		4	1.5–1.8	5,240	1,155	0.075
PEG	*P*1	1	1.78-∞	39,064	27,570	0.190§
PEG	$P2_1$	1	2.49-∞	18,559	14,134	

*The 4–4–20 Fab/fluorescein complex was crystallized in 47% (v/v) MPD and in 16% (w/v) PEG-3350. Space groups were initially determined using 8° or 10° precession photos, although the lattice parameters used for structure determination were obtained from diffractometer data.

‡Diffraction data were collected with a Siemens-Nicolet P21 diffractometer using an omega step scan procedure (Wyckoff et al., 1967) and intensities were corrected for background, absorption, and radiation damage as described previously (Edmundson et al., 1972). Four crystals were used to collect the data sets for the MPD form. Data sets were merged by scaling common shells (6.5-Å to ∞) for the four crystals. Inter-crystal *R* values (R_m) for these mergings are shown in the column on the right. R_m is defined as $R_m = \sum |\,|F_1| - |F_2|\,| / \sum |F_1|$, where $|F_1|$ and $|F_2|$ are the observed structure factor amplitudes for the 6.5-Å to ∞ shells of the two data sets being merged. The PEG triclinic form was particularly resistant to radiation damage, and only one crystal was required for data collection. One crystal was sufficient for the PEG monoclinic form, but the data extended only to 2.5-Å resolution.

§ The *R* value (R_f) comparing the two triclinic data sets (PEG-*P*1 vs. MPD-*P*1) is defined as $R_f = \sum |\,|F_{mpd}| - |F_{peg}|\,| / \sum |F_{mpd}|$, where $|F_{mpd}|$ and $|F_{peg}|$ are the observed structure factor amplitudes of the MPD and triclinic PEG forms, respectively. It was computed over a resolution range of 1.78 Å to infinity.

our computer graphics workstations); and 2) the general immunoglobulin numbering scheme described by Kabat et al. (1991). The latter was used throughout the text. It should be mentioned that Kabat's numbering of the third complementarity-determining region of the heavy chain (H3) was different than that described by Bedzyk et al. Specifically, Bedzyk et al. used the numbers 100a-100d for the sequence YYGM, while Kabat et al. used the numbers 96–99. Amino acid sequences for the constant domains (C_L and C_H1) were taken from Kabat et al. (1991). A consensus sequence based on 11 murine κ light chains (Nos. 11–21) was used for the C_L domain, and a consensus sequence was taken from four murine IgG2a antibodies (Nos. 92–95) for the C_H1 domain.

Refinement of the MPD structure

The MPD structure was refined from 2.7–1.75-Å by simulated annealing with X-PLOR (Brünger et al., 1987) and water molecules were added. Their positions were identified in F_o-F_c maps, which were calculated using phases from the 1.75-Å model. The maps were contoured at the 3 σ(ρ) level, where σ is the standard deviation and ρ is the electron density. Water molecules were only assigned to peaks that were more than 2.5 Å away from the protein. Next, the solvated structure was refined by simulated annealing and re-examined using both F_o-F_c OMIT maps (Bhat and Cohen, 1984) and $2F_o$-F_c maps. OMIT maps were contoured at the 3σ (ρ) level and $2F_o$-F_c maps were contoured at the 2σ (ρ) level. Only water molecules that satisfied the following three criteria were retained in the model: 1) electron density was observed in both types of maps; 2) the nearest neighboring atom was at least 2.5 Å away; and 3) at least one hydrogen bond (or other electrostatic interaction) was formed between the water molecule and its neighbors. Also, maps were searched for unassigned solvent density that had been missed on the first pass. This cycle was repeated until the number of solvent molecules stabilized at 297. Once the structure was solvated, restrained least-squares refinement with PROLSQ (Hendrickson and Konnert, 1981) was used to produce the final structure with optimized stereochemistry. The results of the final refinement are presented in Table 3. An F_o-F_c OMIT map of the antigen-combining site is shown in the top panel of Fig. 3. In our original 2.7-Å structure of the MPD form, we had placed an MPD molecule into unassigned electron density that was located deep within the antigen-combining site (Herron et al., 1989). Interestingly, after refinement at 1.75-Å this electron density seemed more appropriate for two water molecules (W27 and W65), which were substituted for MPD.

Refinement of the PEG structures

Once the MPD structure was completed, we used it as a starting model for molecular replacement studies with the triclinic PEG data set. These studies confirmed our hypothesis that the Fab had the same orientation within the unit cell in both triclinic crystal forms (MPD and PEG). Following molecular replacement, the triclinic PEG structure was re-

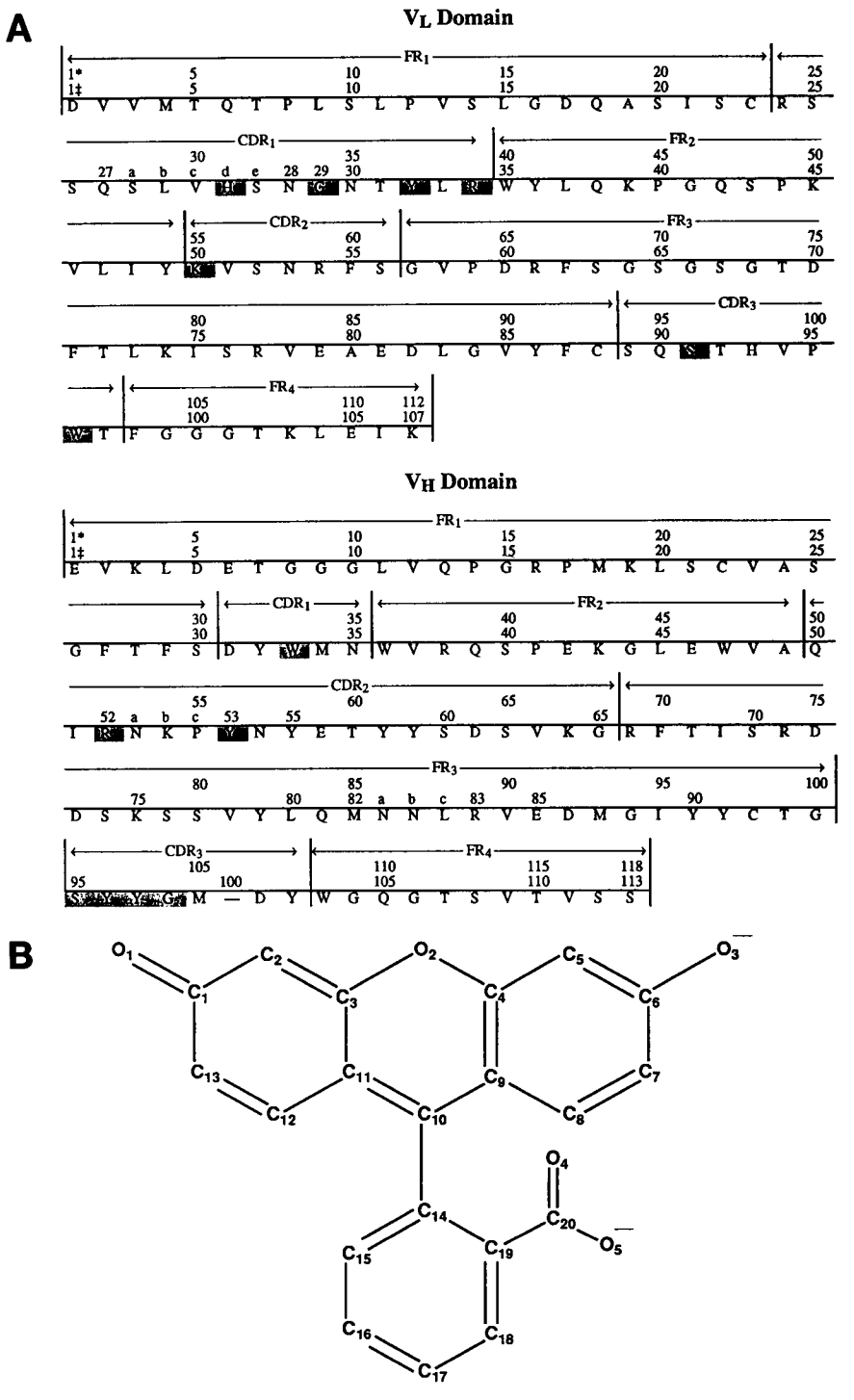

FIGURE 2 (*A*) Amino acid sequences of the "variable" domains of the light and heavy chains (V_L and V_H) of the 4–4–20 antibody, as deduced from nucleotide sequences by Bedzyk et al. (1989, 1990a). (*) The strict sequential numbering system used in our computer graphics workstations. (‡) A general numbering scheme introduced for immunoglobulins by Kabat et al. (1991). The latter number scheme was used throughout the text. Framework (FR) and complementarity-determining regions (CDR) are denoted above the sequence numbers. Key contact residues in the antigen-combining site are highlighted. (*B*) Chemical structure of fluorescein with atom labels. This labeling scheme was used throughout the text.

fined to 1.78-Å resolution and solvated with 287 water molecules as described above. Refinement results are presented in Table 3, and an F_o-F_c OMIT map of the antigen-combining site is shown in the middle panel of Fig. 3.

The 1.78-Å structure of the triclinic PEG form was then employed as the starting model for studies with the monoclinic PEG data set. These studies confirmed that the orientation of the Fab fragment in the *ac* plane of the monoclinic structure was nearly identical to the orientation found in the *ab* plane of the triclinic structure (Fig. 4). Thus, the two PEG forms appeared to be packing variants of each other. The monoclinic PEG model was refined to 2.49-Å resolution and solvated as described above. Refinement results are presented in Table 3, and an F_o-F_c OMIT map of the antigen-combining site is shown in the bottom panel of Fig. 3. A total of 179 water molecules were assigned, ~38% fewer than observed for the triclinic PEG structure.

TABLE 3 Summary of refinement results*

Protein crystal form space group	4-4-20 Fab/fluorescein MPD *P*1	 PEG *P*1	 PEG $P2_1$	
Resolution limits (Å)	1.75–6.0	1.78–6.0	2.49–6.0	
Number of reflections	24,700	26,297	12,114	
R value‡	0.207	0.214	0.184	
Coordinate error (Å)§				
(Luzzati)	0.20–0.25	0.20–0.25	0.25	
(Cruickshank)	0.24	0.25	0.30	
Average temperature factor (Å^2)	15.5	18.5	19.5	
Number of water molecules	297	287	179	
	Actual RMS deviation			Target
rms deviations from ideal distance (Å)				
Bond distance	0.016	0.017	0.015	0.020
Angle distance	0.034	0.034	0.036	0.030
Planar 1–4 distance	0.039	0.038	0.039	0.040
Hydrogen bonds¶	0.042	0.044	0.046	0.050
rms deviation from planarity (Å)	0.020	0.020	0.020	0.025
rms deviation from ideal chirality (Å^3)	0.141	0.143	0.145	0.150
rms deviation from permitted contact distance (Å)				
Single torsion contacts	0.209	0.201	0.208	0.300
Multiple torsion contacts	0.274	0.247	0.281	0.300
Possible hydrogen bond	0.284	0.290	0.269	0.300
rms deviation from ideal torsion angles (°)				
For planar group (0° or 180°)	5.5	6.8	5.2	3.0
For staggered group (±60° or 180°)	22.3	23.0	23.9	15.0
For orthonormal group (±90°)	22.6	26.9	26.2	15.0

*Structures were refined by simulated annealing with X-PLOR. Final refinements were performed with PROLSQ. Weighting factors for PROLSQ were obtained from the equation $\omega = (1/\sigma)^2$, where $\sigma = 15.2–70.0\,[\sin(\theta)/\lambda\text{-}1/6]$ for the MPD structure; $\sigma = 11.6–69.0[\sin(\theta)/\lambda\text{-}1/6]$ for the triclinic PEG structure; and $\sigma = 17.5–129.5[\sin(\theta)/\lambda\text{-}1/6]$ for the monoclinic PEG structure.

‡At 2.0 Å resolution with comparable refinement statistics, the MPD (*P*1) form exhibited an *R* value of 0.196 for 19,808 reflections, and the PEG (*P*1) form exhibited an *R* value of 0.202 for 21,615 reflections.

§Coordinate errors were estimated by two different methods: Luzzati's method for determining the overall rms error of the structure from the variation in *R* value with resolution (Luzzati, 1952) and Cruickshank's formulae for estimating individual coordinate errors from Fourier methods (Cruickshank, 1949, 1950, 1954; Fujinaga et al., 1985). In the latter case, the error for the overall structure was determined by taking the rms average of the individual coordinate errors.

¶Explicit hydrogen bonds for β-pleated sheets.

Comparison of the MPD and PEG triclinic forms

Fig. 5 (*top*) shows a comparison of the C_α skeletal models of the two triclinic structures. They were very similar, even though their antigen-binding affinities differed by more than 20-fold ($\Delta\Delta G° = 1.8$ kcal mol^{-1}, Table 1). For example, the two Fab fragments had nearly the same elbow-bend angles (173.4° and 174.2° for the MPD and PEG forms, respectively). In addition, the rms difference between the two structures for all C_α atoms was 0.71 Å. In another analysis, the C_α traces of the variable domain dimers (V_L-V_H) of the two triclinic structures were superimposed and key contact residues in the antigen-combining site were compared (Fig. 6, *top*). The rms differences between contact residues (all atoms in each contact residue were included in the analysis) varied between 0.28 Å and 0.65 Å for the individual residues, with a combined average of 0.42 Å (Table 4). To assess whether any of these differences were significant, the rms errors in the positions of the contact residues were estimated by the Cruickshank method (Cruickshank, 1949, 1950, 1954; Fujinaga et al., 1985). The results of this error analysis are presented in Table 4 and indicated that only three of the above rms differences (Ser-L91, Ser-H95, Gly-H98) were significant at the 95% confidence level, and only one (Ser-H95) was significant at the 99% level. Although the side chain of Ser-L91 forms a hydrogen bond with fluorescein, the other two residues only make minor contributions to binding (Table 8). Thus, the changes in the positions of these residues are probably not responsible for the observed difference in affinity. This issue will be discussed more thoroughly in a later section.

Although the two triclinic structures were similar, several regions of polypeptide backbone exhibited rms differences >1 Å (Table 5). These regions comprised only about 6% of the total protein structure, but were interesting to examine because they probably represented segments of above average mobility. There was substantial supporting evidence for this suggestion. First, the observed differences were not due to packing interactions because the two triclinic forms were nearly isomorphous. Second, all of the regions were located near the surface of the molecule and were constrained by little, if any, secondary structure. Third, the temperature factors for these regions were 25–50% above average, as is often

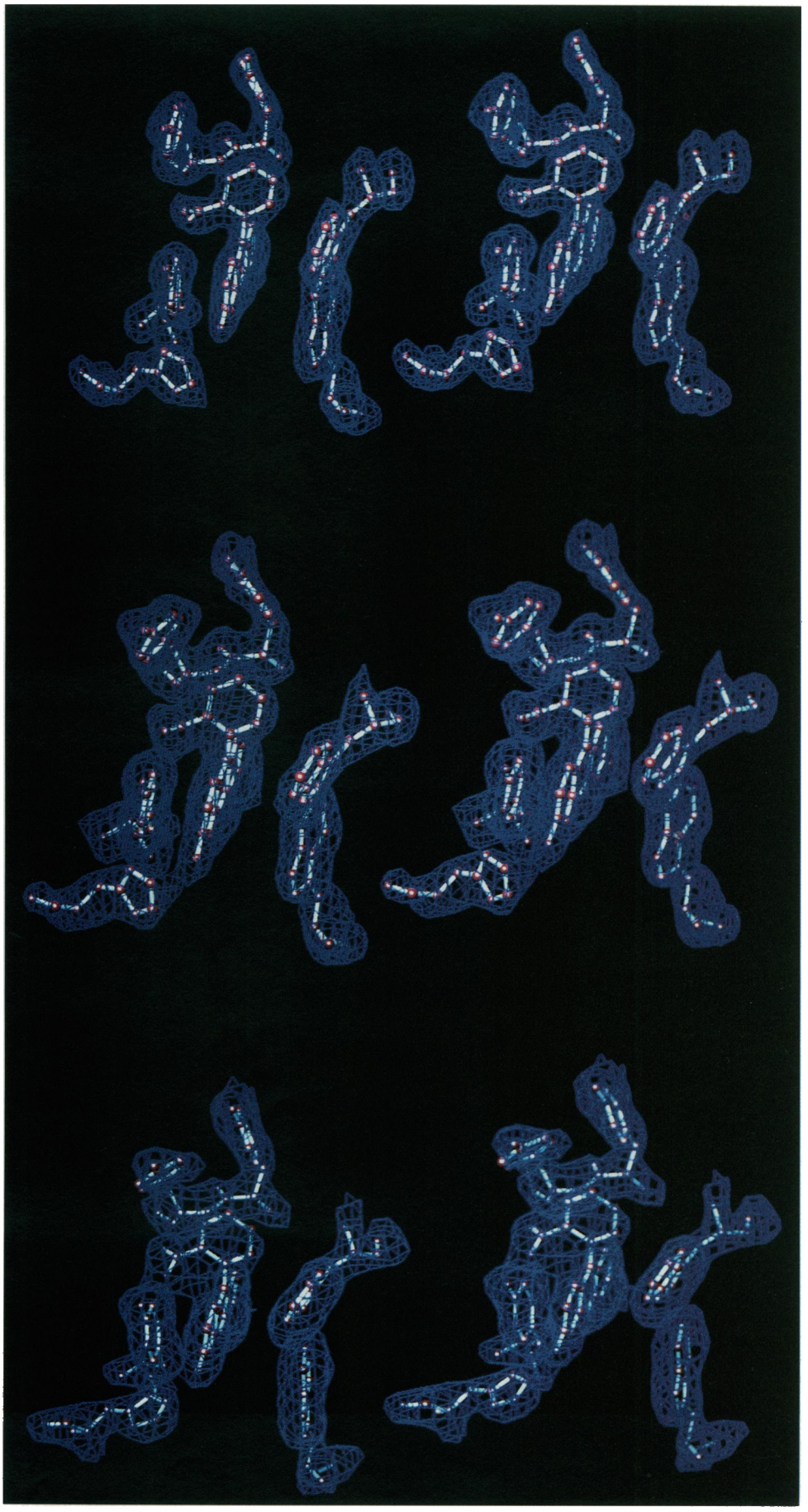

FIGURE 3 Stereo diagram of F_o-F_c OMIT maps for the antigen-combining site of the 4–4–20 Fab/fluorescein complex. All atoms in fluorescein and the following contact residues were deleted from structure factor calculations (F_c): His-L27d, Tyr-L32, Trp-L96, Trp-H33, Tyr-H97, Tyr-H96. Maps were contoured at a level of 2.5σ (ρ), where σ is the standard deviation and ρ is electron density. (*Top*) 1.75-Å structure of the MPD form. Fluorescein is in the center of the photo, with residues His-L27d, Tyr-L32, Tyr-H97, Tyr-H96, Trp-L96, and Trp-H33 (clockwise from bottom left). (*Middle*) 1.78-Å structure of the triclinic PEG form. Pictured residues are the same. (*Bottom*) 2.49-Å structure of the monoclinic MPD form.

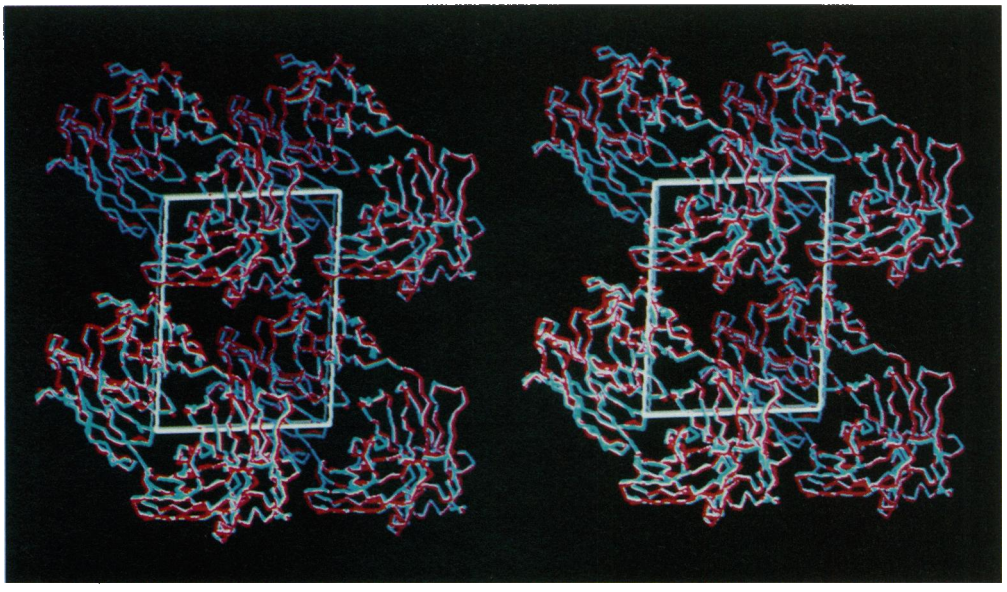

FIGURE 4 Stereo packing diagram comparing the *ab* plane of the triclinic PEG form (blue) to the *ac* plane of the monoclinic PEG form (red).

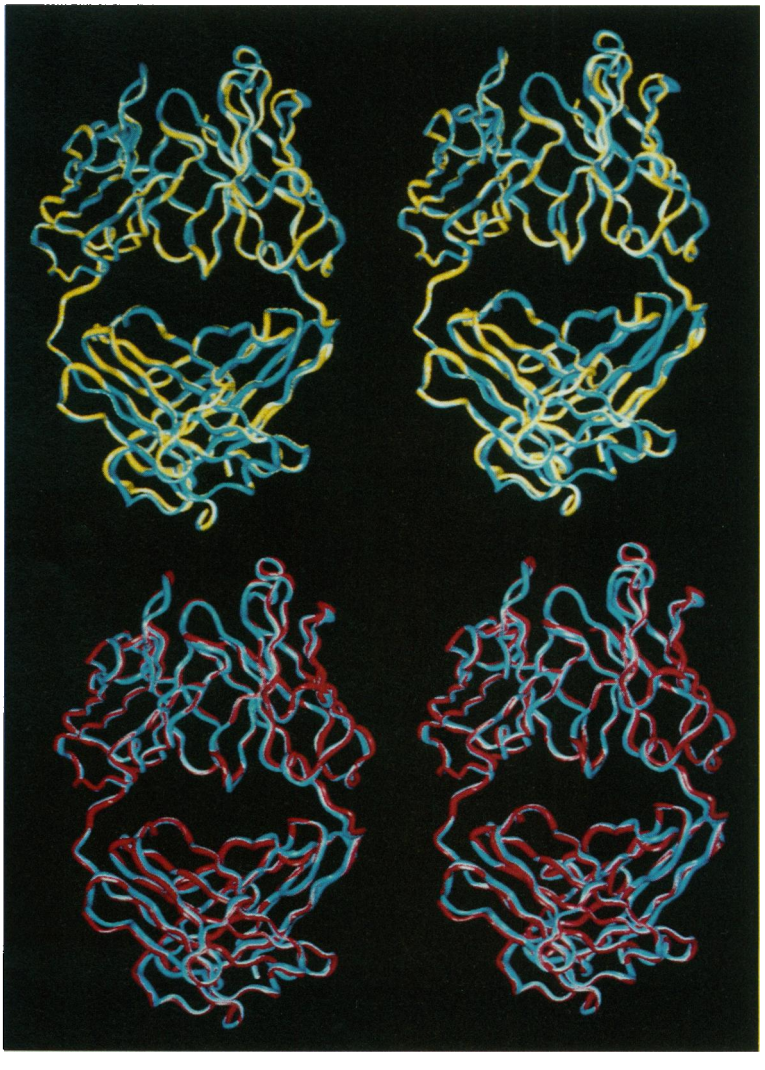

FIGURE 5 Stereo diagrams comparing the C_α traces of different crystal forms of the 4–4–20 Fab/fluorescein complex. (*Top*) comparison of the two triclinic forms. MPD is shown in yellow and PEG is shown in blue. Regions where the two forms overlap exhibit a "calico" appearance. (*Bottom*) comparison of the two PEG forms. Triclinic is shown in blue and monoclinic is shown in red.

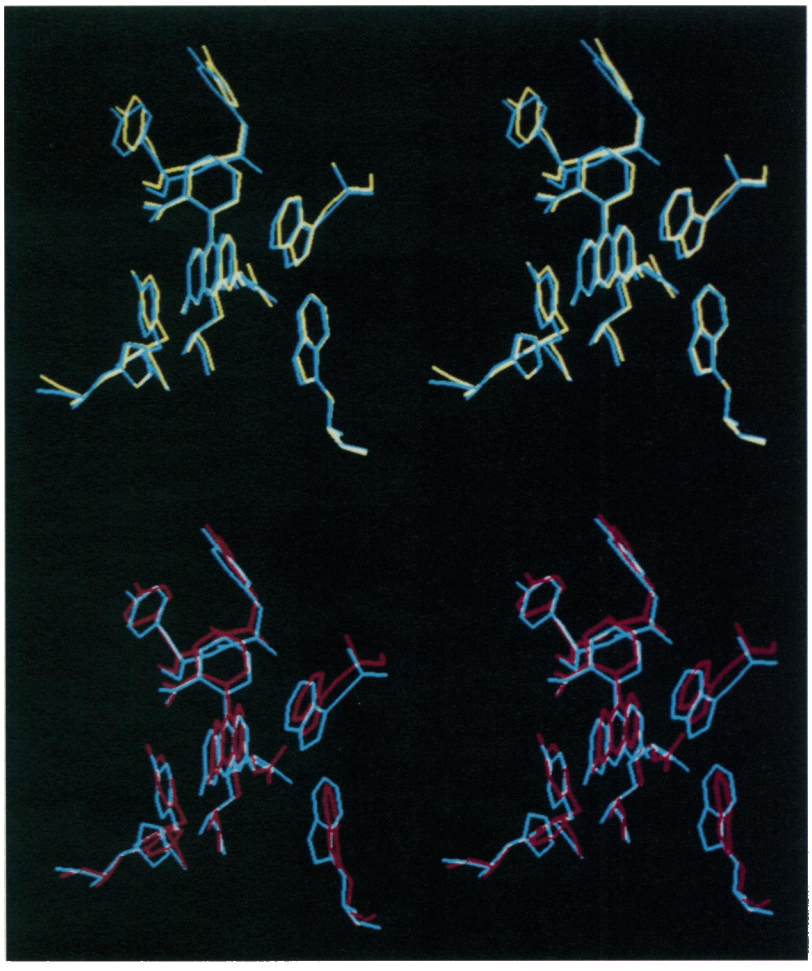

FIGURE 6 Stereo diagrams comparing the tertiary structure of key active site residues in the three crystal forms. (*Top*) comparison of the two triclinic forms. MPD is shown in yellow and PEG is shown in blue. Fluorescein is in the center of the photo, with residues His-L27d, Tyr-L32, Tyr-H97, Tyr-H96, Trp-L96, and Trp-H33 (clockwise from bottom, left). Arg-L34 is located to the rear of fluorescein. (*Bottom*) comparison of the two PEG forms. Triclinic is shown in blue and monoclinic is shown in red. Pictured residues are the same.

observed with mobile surface residues, and the electron density was well defined for these segments. Finally, homologous regions also exhibited above-average mobility in the BV04–01 Fab fragment, which crystallized in a triclinic space group with lattice parameters and Fab orientations similar to those in the MPD form of 4–4–20 (Herron et al., 1991).

Water molecules assigned to the two triclinic structures were similar in number (297 in the MPD form vs. 287 in the PEG form) but differed somewhat in distribution pattern. This distribution was evaluated in two ways. First, the number of hydrogen bonds formed between water molecules and protein constituents was calculated, as well as the number formed between pairs of water molecules. Second, water molecules were classified into two categories: those which were hydrogen bonded to protein constituents, and those which were *only* hydrogen bonded to other water molecules. In essence, water molecules in the former category belonged to the inner hydration shell of the Fab, while those in the latter category did not associate directly with the protein.

The results of these analyses are presented in Table 6 and suggested that the PEG form exhibited a more organized inner hydration shell. For example, it exhibited both a greater number of protein-water hydrogen bonds (287 for PEG vs. 253 for MPD) and a slightly higher number of water molecules which were hydrogen bonded to protein constituents (181 for PEG vs. 175 for MPD). In contrast, the MPD form exhibited higher numbers of both water-water hydrogen bonds (156 for MPD vs. 149 for PEG) and water molecules which were only hydrogen bonded to other water molecules (122 for MPD vs. 106 for PEG). These observations may be due to the different concentrations of precipitants used to grow the two crystal forms; 47% (v/v) MPD is probably more hygroscopic than 16% (w/v) PEG and hence may cause greater disruption of the inner hydration shell of the MPD form. This issue will be examined further in the Discussion.

Comparison of the triclinic and monoclinic PEG forms

The two PEG forms were compared by the methods used to analyze the two triclinic forms. Skeletal C_α models are shown in the bottom panel of Fig. 5, and key contact residues in the antigen-combining site are presented in the bottom panel of Fig. 6. The elbow-bend angle of the monoclinic form (176.0°) is slightly greater than that of the triclinic form (174.2°), but there are no other significant differences in quaternary structure. The rms difference between the two PEG structures was 0.78 Å for all C_α atoms, compared with the value of 0.71 Å for the MPD and PEG triclinic structures. Regions

TABLE 4 Differences in the atomic positions of contact residues in the active sites in the three forms of the 4-4-20 Fab/fluorescein complex

Residue	MPD vs. PEG-P1		PEG-P1 vs. PEG-$P2_1$	
	rms difference* (Å)	rms error‡ (Å)	rms difference* (Å)	rms error‡ (Å)
CDR-L1				
His-L27d	0.30	0.36	0.75	0.39
Gly-L29	0.56	0.43	0.15	0.40
Tyr-L32	0.36	0.25	0.58	0.31
Arg-L34	0.45	0.26	0.81§	0.29
CDR-L2				
Lys-L50	0.40	0.22	0.67§	0.33
CDR-L3				
Ser-L91	0.60§	0.30	0.55	0.32
Trp-L96	0.28	0.29	0.94§	0.33
CDR-H1				
Trp-H33	0.39	0.32	0.73	0.38
CDR-H2				
Arg-H52	0.38	0.31	0.61	0.33
Tyr-H53	0.31	0.39	0.86§	0.38
CDR-H3				
Ser-H95	0.65§	0.25	0.93§	0.34
Tyr-H96	0.47	0.34	0.69	0.40
Tyr-H97	0.48	0.32	0.55	0.40
Gly-H98	0.53§	0.25	0.54	0.33
All contact residues	0.42	0.31	0.72§	0.35

*The C_α traces of the variable domain dimers (V_L-V_H) of the two triclinic structures (MPD vs. PEG-*P*1) were superimposed and key contact residues in the antigen-combining site were compared. Specifically, the root mean square (rms) difference between each contact residue was computed using the following formula:

$$\text{rms difference} = \left(\frac{\sum_i^n (\bar{x}_{1i} - \bar{x}_{2i})^2}{n}\right)^{1/2}$$

where $\bar{x}_{1i}$ represents the atomic coordinates for an atom in the MPD structure, $\bar{x}_{2i}$ represents the coordinates for the same atom in the PEG-*P*1 structure, and n is the total number of atoms in each contact residue. This procedure was repeated with the two PEG structures (PEG-*P*1 vs. PEG-$P2_1$).

‡To assess whether the above rms differences were significant or not, the rms errors in the positions of the contact residues were also determined. Estimated coordinate errors were calculated for all atoms in the contact residues using the Cruickshank formulae (Cruickshank, 1949, 1950, 1954; Fujinaga et al., 1985). Because two structures were being compared (MPD vs. PEG-P1) the combined rms error of each contact residue was computed as follows:

$$\text{rms error} = \left(\frac{\sum_i^n (\sigma_{1i}^2 + \sigma_{2i}^2)}{n}\right)^{1/2}$$

where σ_{1i} is the estimated coordinate error for an atom in the MPD structure, σ_{2i} is the estimated error for the same atom in the PEG-*P*1 structure, and n is the total number of atoms in each contact residue. This procedure was repeated with the two PEG structures (PEG-P1 vs. PEG-$P2_1$).

§The observed rms difference for this residue is significant at the 95% confidence level (rms difference ≥1.96*rms error). This suggests that it occupies different positions in the two crystal forms.

of the two PEG structures differing by >1 Å (rms) are listed in Table 7. These differences were due either to dissimilar packing interactions or to the inherent flexibilities discussed above.

Differences between key contact residues in the antigen-combining site were somewhat larger than observed for the two triclinic structures. The rms differences of individual residues varied between 0.15 and 0.94 Å, with a combined average of 0.72 Å (Table 4). As described above, these differences were compared with the estimated rms coordinate errors of the contact residues. This analysis indicated that five of the rms differences (Arg-L34, Lys-L50, Trp-L96, Tyr-H53, Ser-H95) were significant at the 95% confidence level and three (Arg-L34, Trp-L96, Ser-H95) were significant at the 99% level. Considering that both Arg-L34 and Trp-L96 make important contributions to the electrostatic character and shape of the antigen-combining site, it is not surprising that fluorescein occupies slightly different positions in the two PEG structures (Fig. 6, *bottom*). These differences are probably due to the dissimilar packing interactions and/or different resolution levels of the two structures.

Other prominent differences involved the solvent structures. Fewer water molecules were assigned to the monoclinic form than to the triclinic form (179 vs. 287). In addition, the monoclinic form had fewer water molecules hydrogen bonded to protein constituents than the triclinic form (99 in the monoclinic vs. 181 in the triclinic; Table 6), and fewer than half as many solvent-protein hydrogen bonds (131 for monoclinic vs. 287 for triclinic). The monoclinic structure also exhibited fewer water-water hydrogen bonds than the triclinic structure (61 vs. 149). These comparisons are of limited value, however, in trying to evaluate the water structure of the two crystal forms because of the lower resolution of the monoclinic form.

Fluorescein binding site

Practically all features previously described for the fluorescein binding site (Herron et al., 1989) were found in the three present structures. To ascertain whether any other novel features could be identified in the binding site at higher resolution, we calculated the potential energies of fluorescein with neighboring residues (Table 8). This analysis showed that several residues located in the second and third CDRs of the heavy chain and the second CDR of the light chain had a greater role in binding fluorescein than we had supposed. A new van der Waals interaction was observed between the phenolic group of Tyr-H53 (located in H2) and fluorescein's xanthenone ring (Table 8). Specifically, atoms CE2 and OH of Tyr-H53 made contact with atoms C_{12} and C_{13} of fluorescein. Since Tyr-H53 was located near the entrance to the slot (in front of Trp-H33, and to the right of His-L27d), it helped to shield the xanthenone ring from solvent. Direct evidence for this effect was found in the two PEG structures; a water molecule (W192) was located within hydrogen bonding distance of Tyr-H53's hydroxyl group in the triclinic form and two such water molecules (W126 and W127) were observed in the monoclinic form. A new electrostatic interaction was observed between the guanido group of Arg-H52 and fluorescein's O_1 enolic group. Arg-H52 was located on the right side of the site, immediately below Tyr-H53. Located 5 Å away from fluorescein, Arg-H52 was not a contact residue, but did contribute to the overall electropositive character of the antigen-combining

TABLE 5 Differences in tertiary structure between the MPD and PEG triclinic forms

Region	C_α displacement (Å) rms	Maximum	Comments
Light			
L1-L2* [L1-L2]‡ (DV)§	0.99	1.16	N-terminus of the light chain. The first two residues have slightly different Φ and Ψ angles in the two crystal forms.
L152-L158 [L157-L163] (GSERQNG)	2.01	2.85	Extended region of polypeptide which runs perpendicular to the long axis of the C_L domain. It is located on the external face of the domain, near the carboxyl end. The tertiary structure of the SERQN sequence is essentially the same in the two crystal forms, but the two glycines allowed the MPD form to shift about 2.2 Å relative to the PEG form.
Heavy			
H1-H4 (EVKL)	2.27	3.52	N-terminal segment of the heavy chain. The first two residues occupy different positions in the two crystal forms due to rotations about the Ψ angles of H2 and H3 and the Φ angle of H4.
H62-H65 [H65-H68] (SVKG)	1.20	1.42	Extended, flexible region which connects CDR-H2 to a strand of β-pleated sheet.
H128-H134 [H133-H139] (CGDTTGS)	1.40	2.51	Extended loop which forms the heavy chain half of the interchain disulfide.

*Immunoglobulin numbering scheme of Kabat et al. (1991).
‡Strict sequential number system used in our computer graphics workstations.
§Amino acid sequence.

site. We speculate that it could also be important in directing the fluorescein into the active site.

Several new van der Waals interactions were observed between fluorescein's phenylcarboxylate group and the phenolic groups of both Tyr-H96 and Tyr-H97 (located in H3). Specifically, atoms CD1 and CE1 of Tyr-H96 made contact with atom C_{17} of fluorescein's phenyl ring. Atoms CD1 and CE1 of Tyr-H97 made contact with fluorescein's phenyl ring (C_{18} and C_{19}) and its phenylcarboxylate group (C_{20}, O_4, O_5). Potential energy calculations suggested a dipole-induced dipole interaction between the peptide amino group (NH) of Tyr-H97 and fluorescein's phenyl ring. Finally, the polypeptide backbone of the residues which flank tyrosines H96 and H97 (Ser-H95 and Gly-H98) also made van der Waals contacts with fluorescein. In our original structure, the side chains of Tyr-H96 and Tyr-H97 pointed toward fluorescein's phenylcarboxylate group, but did not make contact with it. Together, these binding site components shield fluorescein from bulk solvent more effectively than previously believed.

The 2.7-Å study (Herron et al., 1989) indicated that only one of fluorescein's two negative charges was formally neutralized on complexation (salt link between Arg-L34 and fluorescein's O_3 enolic group). The second negative charge on fluorescein's phenylcarboxylate group was partially neutralized by a hydrogen bond with Tyr-L32. Lysine-L50 (located in L2) was apparently too far away (5.5 Å) for a strong electrostatic interaction with the phenylcarboxylate. However, our potential energy calculations showed that there was a favorable electrostatic interaction between Lys-L50 and fluorescein (−2.9 to −4.6 kcal/mol; Table 8). Like Arg-H52, Lys-L50 was

TABLE 6 Hydrogen bonds with solvent molecules

Type of hydrogen bond	Number of hydrogen bonds* MPD-*P*1	PEG-*P*1	PEG-$P2_1$
Main chain			
N—H-Water	39	48	13
C=O-Water	74	86	40
Side chain			
Arg-Water	19	12	7
His-Water	5	5	4
Lys-Water	20	24	8
Asp-Water	14	16	12
Glu-Water	9	12	11
Asn-Water	12	15	3
Gln-Water	9	8	8
Ser-Water	29	35	13
Thr-Water	17	19	7
Trp-Water	3	1	1
Tyr-Water	3	6	4
Total protein-water hydrogen bonds:	253	287	131
Total water-water hydrogen bonds:	156	149	61
	Location of water molecules‡		
Number of water molecules hydrogen bonded to protein	175	181	99
Number of water molecules only hydrogen bonded to other waters	122	106	80

*The number of hydrogen bonds between water molecules and protein constituents was tallied for each of the three crystal forms (MPD-*P*1, PEG-*P*1, PEG-$P2_1$). Data were tabulated for hydrogen bonds between solvent molecules and main chain amide and carbonyl groups, as well as for those between solvent molecules and the side chains of polar residues.
‡The number of water molecules that form hydrogen bonds with protein constituents was listed for each of the crystal forms, and the number of waters that were only hydrogen bonded to other water molecules was also determined.

TABLE 7 Differences in tertiary structure between the monoclinic and triclinic PEG forms

Region	C_α displacement (Å) rms	Maximum	Comments
Light			
L14-L17* [L14-L17]‡ (SLGD)§	0.94	1.05	Packing interactions with H52b and H55 in triclinic form and with H65-H66 and H82b in the monoclinic form.
L152-L157 [L157-L162] (GSERQN)	1.55	2.36	Packing interactions with H8-H11 and H151 in the triclinic form, and with H6-H7 and H106-H107 in the monoclinic form.
L213-L214 [L218-L219] (EC)	1.43	1.56	Light chain half of the interchain disulfide bond. Packing interactions with L52 and L54 in both crystal forms.
Heavy			
H1-H3 (EVK)	1.04	1.29	N-terminus of heavy chain. Slightly different Φ and Ψ angles in the first three residues of the two crystal forms.
H25-H27 (SGF)	1.10	1.30	Flexible region adjacent to H1-H3; these two regions move in concert.
H41-H44 (PEKG)	1.45	1.70	Packing interaction (salt link) between Glu H42 and LysH 75 in both crystal forms.
H64-H65 [H67-H68] KG	1.27	1.41	Packing interactions with L14-L15, L106-L107 and L168-L171 in the monoclinic form and with L200-L201 in triclinic form.
H113-H115 [H118-H120] (SAK)	1.15	1.21	Switch region peptide between the V_L and C_H1 domains. Difference is probably due to small changes in the elbow bend angles (~2°) and pseudo-twofold angles (2–3°).
H130-H137 [H135-H140] (DTTGSS)	1.47	1.94	Extended loop near the heavy chain half of the interchain disulfide. Packing interactions with H15-H16 in triclinic form and with H52c-H53 in monoclinic form.
H178-H180 [H175-H177] (LQS)	1.09	1.19	Reverse turn adjacent to H113-H115; the two regions move in concert.
H193-H200 [H188-H194] (VTSSTWP)	2.02	2.99	Packing interactions with L27e-L28 in monoclinic form. Also, this region is adjacent to H130-H137 and moves in concert.

*Immunoglobulin numbering scheme of Kabat et al. (1991).
‡Strict sequential number system used in our computer graphics workstations.
§Amino acid sequence.

not a contact residue, but contributed to the electropositive nature of the site, helping to mask the negative charge on the phenylcarboxylate group.

Phenylcarboxylate also participated in several interesting solvent interactions. In both triclinic structures, a bound water molecule (W22 in the MPD form, W49 in the PEG form) bridged the distance between NZ of Lys-L50 and O_5 of the phenylcarboxylate group, and either one or two water molecules (W23 in the MPD form, W159 and W192 in the PEG form) were hydrogen bonded to atom O_4 of the phenylcarboxylate group. Although these solvent interactions were not observed in the monoclinic PEG form, two water molecules (W126 and W127) located in the vicinity of the phenylcarboxylate group were observed to hydrogen bond to the OH group of Tyr-H53 instead. In summary, the negative charge on the phenylcarboxylate group was partially neutralized by three types of interactions: 1) the hydrogen bond with Tyr-L32; 2) an electrostatic interaction with Lys-L50; and 3) electrostatic interactions with solvent molecules.

DISCUSSION

Lower affinity of the MPD form

At first we thought that the lower affinity of 4–4–20 for fluorescein in MPD would be reflected in the structure of the active site (Gibson et al., 1988). However, since the structures of the sites in the triclinic MPD and PEG forms were nearly identical (Tables 4 and 8, Fig. 6), other factors had to be involved. We suggest that the observed difference in affinity is mainly due to the depletion of the hydration shell of the antigen-combining site. In support of this hypothesis, the MPD structure was found to contain fewer ordered solvent molecules in the antigen-combining site than observed in the triclinic PEG structure. Table 9 shows that the MPD form

TABLE 8 Potential energy of non-bonded interactions between fluorescein and contact residues of 4–4–20

	Potential energy* (kcal mol^{-1})								
	MPD-*P*1			PEG-*P*1			PEG-$P2_1$		
Contact residue	VDW	Elec	Total	VDW	Elec	Total	VDW	Elec	Total
CDR-L1									
His-L27$_d$	1.2	−33.8	−32.7	0.6	−33.4	−32.8	−2.3	−27.2	−29.5
Gly-L29	−0.3	−1.0	−1.3	−0.4	−1.6	−2.0	−0.4	−0.6	−1.0
Tyr-L32	−8.7	−12.7	−21.3	−6.4	−10.3	−16.7	−8.6	−11.2	−19.8
Arg-L34	−1.4	−41.0	−42.4	−1.0	−40.3	−41.3	0.2	−36.7	−36.5
CDR-L2									
Lys-L50	−0.1	−4.6	−4.7	−0.1	−2.9	−3.0	−0.1	−4.1	−4.2
CDR-L3									
Ser-L91	1.2	−11.0	−9.8	0.2	−3.7	−3.5	−1.5	5.2	3.7
Trp-L96	−3.0	0.0	−3.0	−2.9	−0.1	−3.0	−1.2	0.0	−1.2
CDR-H1									
Trp-H33	−7.9	−0.4	−8.3	−9.7	−1.1	−10.8	−10.2	−1.1	−11.4
CDR-H2									
Arg-H52	−0.3	−2.6	−2.9	−0.3	−2.4	−2.7	−0.3	−1.9	−2.2
Tyr-H53	−1.8	−1.5	−3.3	−2.5	−0.4	−2.8	−1.5	2.8	1.3
CDR-H3									
Ser-H95	−1.9	−0.5	−2.3	−1.9	−1.3	−3.2	−1.3	−2.3	−3.5
Tyr-H96	−1.9	−3.6	−5.5	−4.2	−2.2	−6.4	−3.7	−3.5	−7.2
Tyr-H97	−2.0	−15.2	−17.2	−7.5	−13.4	−20.9	−3.0	−14.5	−17.5
Gly-H98	−2.8	−0.7	−3.5	−1.4	−2.6	−4.1	−2.2	−5.7	−7.8
Total for all contact residues	−29.8	−128.5	−158.4	−37.5	−115.7	−153.2	−36.1	−100.7	−136.8

*Potential energies of non-bonded interactions between fluorescein and neighboring residues in the antigen-combining site were calculated using X-PLOR (Brünger et al., 1987). Values were reported for van der Waals (VDW) and electrostatic (Elec) interactions. The sum of these two energies (total) was also reported for each contact residue.

TABLE 9 Potential energy of non-bonded interactions between fluorescein and solvent

	Potential energy* (kcal mol^{-1})										
	MPD-*P*1				PEG-*P*1				PEG-$P2_1$		
Water no.	VDW	Elec	Total	Water no.	VDW	Elec	Total	Water no.	VDW	Elec	Total
22	0.2	−16.1	−15.9	30	−1.1	−8.9	−9.9	42	−0.3	−2.4	−2.7
23	−0.1	−15.0	−15.1	49	−0.1	−16.9	−17.0	126	−0.1	−0.9	−0.9
214	−0.3	−5.9	−6.2	79	−0.3	−4.1	−4.4	127	−1.4	−11.9	−13.2
				159	−0.2	−15.7	−15.9				
				192	−1.6	−13.0	−14.6				
				208	0.0	−0.7	−0.8				
				209	−0.2	−2.0	−2.3				
				210	−0.2	−3.0	−3.2				
	−0.2	−37.0	−37.2		−3.6	−64.3	−68.0		−1.7	−15.1	−16.9

*Potential energies of non-bonded interactions between fluorescein and solvent molecules in the vicinity of the antigen-combining site were calculated using X-PLOR (Brünger et al., 1987). Values were reported for van der Waals (VDW) and electrostatic (Elec) interactions. The sum of these two energies (total) was also reported for each solvent molecule.

contains only three water molecules which exhibited a favorable non-bonded potential energy with the fluorescein-combining site complex (total potential energy of −37.2 kcal mol^{-1}). In contrast eight such water molecules were identified in the triclinic PEG structure (−68.0 kcal mol^{-1}) (see Fig. 7 for illustrations of the solvated antigen-combining sites of both triclinic structures). Although potential energies reflect the internal energy of the antigen-antibody interaction rather than the free energy, they are still useful in assessing the relative contributions of different structural elements to the overall interaction. Considering that the total potential energy of non-bonded interactions between fluorescein and protein was −156 ± 4 kcal mol^{-1} for the two triclinic structures, the additional solvent contribution of −30.8 kcal mol^{-1} in the PEG form suggested that this structure should have a higher affinity. Finally, the observation that the af-

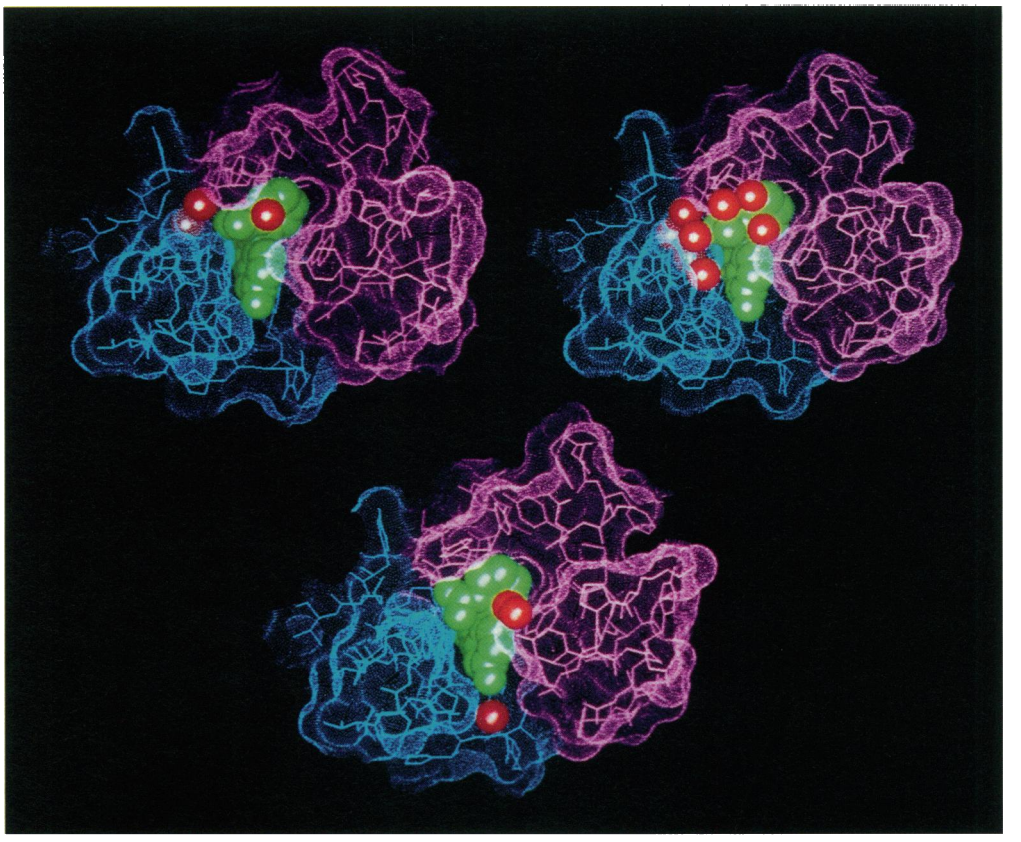

FIGURE 7 Solvation of the antigen-combining sites of the three crystal forms. Solvent-accessible surfaces were calculated as described by Connolly (1983). Light chain residues were colored blue and heavy chain residues magenta. The solvent molecules listed in Table 9 were shown as solid red spheres. Fluorescein is depicted as a green CPK model. (*Top left*) triclinic MPD form; (*top right*) triclinic PEG form; (*bottom*) monoclinic PEG form.

finity of 4–4–20 decreased monotonically with increasing MPD or PEG concentration (Fig. 1) strongly suggested that affinity was inversely related to the hydration properties of the precipitant. With increasing concentration, the hygroscopic molecules of MPD or PEG progressively pull water away from the protein and into their own hydration shells. This phenomenon leads to precipitation (and crystallization) of the Fab fragment but also lowers its affinity, apparently without major changes in the protein structure.

Buried surface area

Several studies have shown that buried surface area is correlated to the hydrophobic effect, especially for buried nonpolar surfaces (Chothia, 1974; Eisenberg et al., 1984; Guy, 1985; Rose et al., 1985; Kellis et al., 1989; Spolar et al., 1989; Makhatadze and Privalov, 1990; Privalov and Makhatadze, 1990; Sharp et al., 1991). Furthermore, there is a conversion factor that relates nonpolar surface area to the component of the free energy change attributable to the hydrophobic effect. Typically, such values range from -16 to -31 cal mol^{-1} Å^{-2}, with an average of about -25 cal mol^{-1} Å^{-2} (Sharp et al., 1991). Davies et al. (1990) reported that buried surface area ranged from 300 to 1700 Å^2 in a series of antigen-antibody complexes including our 4–4–20 Fab/fluorescein complex at 2.7-Å resolution. We extended such computations to the three new structures and modified the approach to include the fraction of buried surface area involving nonpolar constituents. These values are listed in Table 10. The average total buried surface area in the three forms was 585 $\pm$ 8 Å^2, of which 338 $\pm$ 12 Å^2 (58%) was due to nonpolar atoms. The free energy change due to the hydrophobic effect was calculated to be -8.5 ± 0.3 kcal mol^{-1} (Table 10). As measured by fluorescence quenching assay (Herron, 1984), the empirical $\Delta G°$ value for the 4–4–20/fluorescein complex was -13.9 kcal mol^{-1} at 25°C (Herron et al., 1986; Gibson et al., 1988).

We interpret these results to imply that the aromatic binding cavity possesses a fundamental free energy of interaction of about -8 to -9 kcal mol^{-1} due to the hydrophobic effect. For promotion of complexation, the hydrophobic effect is augmented by non-bonded interactions through van der Waals contacts, hydrogen bonds, and salt links between fluorescein and residues in the binding cavity. Moreover, electrostatic interactions (hydrogen bonds, salt links) that form between fluorescein and buried polar groups may be significantly stronger than comparable interactions in bulk solvent because of the low dielectric constant within the binding cavity. If the correlation between buried nonpolar surface area and hydrophobic free energy is valid, then non-bonded

TABLE 10 Buried surface area of the 4–4–20 Fab/fluorescein complex and calculated hydrophobic components of heat capacity and free energy

Structural moiety	Polarity	Buried surface area (Å²)* MPD-P1	PEG-P1	PEG-P2₁	Average
Binding site	Polar+nonpolar	315	309	314	313±3
Binding site	Nonpolar	162	145	148	152±9
Fluorescein	Polar+nonpolar	279	271	266	272±7
Fluorescein	Nonpolar	190	187	183	187±4
Complex	Polar+nonpolar	594	580	580	585±8
Complex	Nonpolar	352	332	331	338±12
		Calculated hydrophobic components‡			
$\Delta G^\circ_{(hydro)}$	(kcal mol^{-1})	−8.8	−8.3	−8.3	−8.5±0.3
$\Delta C_p{}^\circ_{(hydro)}$	(cal mol^{-1} °K^{-1})	−99	−93	−93	−93±3

*Buried surface area was computed for the three crystal forms of the 4–4–20 Fab/fluorescein complex as described previously (Davies et al., 1990). Values were reported for: 1) the antigen-combining site without fluorescein (binding site); 2) free fluorescein (fluorescein); and 3) the Fab/fluorescein complex (complex). In addition, values were determined for total buried surface area (polar + nonpolar) and nonpolar buried surface area (nonpolar). The average buried surface area for the three crystal forms was reported in the rightmost column.

‡The contributions of the hydrophobic effect to the free energy of binding [$\Delta G^\circ_{(hydro)}$] and the change in heat capacity [$\Delta C_p{}^\circ_{(hydro)}$] were calculated as described previously (Sharp et al., 1991). A conversion factor of −25 cal mol^{-1} Å^{-2} was used to relate nonpolar, buried surface area to the free energy of binding, while that of −0.28 cal mol^{-1} °K^{-1} Å^{-2} was used to compute the heat capacity change.

interactions are probably responsible for ~−5 kcal mol^{-1} of the binding energy. The 3-D structures indicate the formation of the three hydrogen bonds and one salt link during complexation. One of these hydrogen bonds and the salt link could together account for about −4.5 kcal mol^{-1} of the binding energy (Omelyanenko et al., 1993). Thus, electrostatic interactions probably play important roles in the complexation of 4–4–20, as well as in the formation of other antigen-antibody complexes of high affinity.

Induced-fit in 4–4–20

The above interpretations were made without considering possible changes in the conformational entropy or vibrational modes of the antigen and antibody. Immunologists have long been interested in whether antigens and antibodies form complexes between two static partners ("lock and key" mechanism) or whether they can change their conformations to achieve greater complementarity ("induced-fit" hypothesis) (Berzofsky, 1985). In lock and key mechanisms, the change in conformational entropy of the antibody should be minimal because the structure of the antigen-combining site does not change upon binding. Formation of the complex by an induced-fit mechanism, however, "locks" both partners into a single conformational state. Both conformational and vibrational entropy may therefore be significantly lower for the antigen-antibody complex than for the unbound state. An induced-fit mechanism should lead to an increase in the diversity of antigens to which a particular antibody can respond. However, it is an energetically unfavorable process and probably takes place at the expense of other more favorable interactions.

Although the native (unliganded) form of the 4–4–20 Fab has not been crystallized, several lines of evidence suggest that an induced-fit mechanism may be involved in the binding of fluorescein. First, kinetic studies indicated a two-step association reaction—a second-order collision event followed by a first-order accommodation step (Kranz et al., 1982; Herron, 1984). Second, thermodynamic studies suggested that the binding of fluorescein may be accompanied by a loss in vibrational entropy (Herron et al., 1986). This conclusion was based on the work of Sturtevant (1977), who reported that the entropy change in many protein-ligand interactions at 25°C was much lower than predictions based on the hydrophobic effect. He suggested that the discrepancy may be due to a loss in the vibrational entropy of the protein upon binding.

Third, time-resolved fluorescence anisotropy studies indicated that the hydrodynamic behavior of the 4–4–20 Fab changed upon formation of the Fab/fluorescein complex (Lim et al., submitted for publication). Specifically, the liganded Fab was shown to have a smaller hydrodynamic volume and less segmental flexibility (i.e., to be more rigid) than the unliganded form. These observations were consistent with the results of molecular dynamics (MD) simulations of the 4–4–20 Fab, performed in the presence and absence of fluorescein, which had been undertaken to study the structural aspects of the induced-fit mechanism in 4–4–20 (Lim and Herron, submitted for publication). These simulations also suggested that the antigen-combining site collapsed during the first 4 ps of the simulation, after fluorescein was removed from the site using a simulated pulling force. After the initial collapse, the site gradually reformed during the next 100 ps of the simulation. Motions of the two tryptophan residues (L96 and H33) were primarily responsible for the collapse, although the side chain of Tyr-H53 also moved. The movement of Trp-L96 was transmitted to the rest of the β-strand to which it was attached (L96-L104). Although these results are merely predictions based on MD simulations, they do suggest that dissociation of fluorescein from the antigen-combining site is accompanied by movements in both the side chains and main chains of certain contact residues.

Finally, the failure of the unliganded Fab to crystallize under the same conditions as the liganded Fab suggested that the unliganded and liganded forms may have a significantly different conformations. This premise is supported by the observation that polyclonal antibodies elicited against the 4–4–20/fluorescein complex were found to bind exclusively to the liganded forms of the 4–4–20 IgG, its Fab fragment and a recombinant single chain antibody derivative, but exhibited little if any activity for the unliganded forms of these

species (Weidner and Voss, 1991). This phenomenon has been termed "metatypy" and may be generally operable in immune recognition (Voss, 1990). In our combined laboratories the most familiar precedents for these suggestions are the antigen-induced changes in the BV04–01 Fab (Herron et al., 1991).

We thank Dr. Steven Sheriff (Bristol-Myers Squibb) for providing his programs for computing estimated coordinate errors and buried surface areas, Silicon Graphics for gifts of graphics workstations, and BIOSYM Technologies for supplying their Insight II and Discover programs.
This work was supported by National Institutes of Health Grants AI 22898 (to J.N.H.) and CA 19616 (to A.B.E.), by the Utah Supercomputing Institute (to J.N.H), and by the Harrington Cancer Center (to A.B.E.).

REFERENCES

Altschuh, D., O. Vix, B. Rees, and J.-C. Thierry. 1992. A conformation of cyclosporin A in aqueous environment revealed by the x-ray structure of a cyclosporin-Fab complex. *Science*. 256:92–94.

Alzari, P. M., S. Spinelli, R. A. Mariuzza, G. Boulot, R. J. Poljak, J. M. Jarvis, and C. Milstein. 1990. Three-dimensional structure determination of an anti-2-phenyloxazolone antibody: the role of somatic mutation and heavy/light chain pairing in the maturation of an immune response. *EMBO J.* 9:3807–3814.

Amit, A. G., R. A. Mariuzza, S. E. V. Phillips, and R. J. Poljak. 1986. Three-dimensional structure of an antigen-antibody complex at 2.8-Å resolution. *Science*. 233:747–753.

Arevalo, J. H., E. A. Stura, M. J. Taussig, and I. A. Wilson. 1993. Three-dimensional structure of an anti-steroid Fab′ and progesterone-Fab′ complex. *J. Mol. Biol.* 231:103–118.

Bedzyk, W. D., J. N. Herron, A. B. Edmundson, and E. W. Voss, Jr. 1990a. Active site structure and antigen binding properties of idiotypically cross-reactive anti-fluorescein monoclonal antibodies. *J. Biol. Chem.* 265: 133–138.

Bedzyk, W. D., L. S. Johnson, G. S. Riordan, and E. W. Voss, Jr. 1989. Comparison of variable region primary structures within an anti-fluorescein idiotype family. *J. Biol. Chem.* 264:1565–1569.

Bedzyk, W. D., K. M. Weidner, L. K. Denzin, L. S. Johnson, K. D. Hardman, M. W. Pantoliano, E. D. Asel, and E. W. Voss, Jr. 1990b. Immunological and structural characterization of a high affinity anti-fluorescein single-chain antibody. *J. Biol. Chem.* 265:18615–18620.

Berzofsky, J. A. 1985. Intrinsic and extrinsic factors in protein antigenic structure. *Science*. 229:932–940.

Bhat, T. N., and G. H. Cohen. 1984. OMITMAP: An electron density map suitable for the examination of errors in a macromolecular model. *J. Appl. Crystallogr.* 17:244–248.

Brünger, A. T., J. Kuriyan, and M. Karplus. 1987. Crystallographic R factor refinement by molecular dynamics. *Science*. 235:458–460.

Chothia, C. 1974. Hydrophobic bonding and accessible surface area in proteins. *Nature*. 248:338–339.

Colman, P. M., W. G. Laver, J. N. Varghese, A. T. Baker, P. A. Tulloch, G. M. Air, and R. G. Webster. 1987. Three-dimensional structure of a complex antibody with influenza virus neuraminidase. *Nature*. 326: 358–363.

Colman, P. M., W. R. Tulip, J. N. Varghese, P. A. Tulloch, A. T. Baker, W. G. Laver, G. M. Air, and R. G. Webster. 1989. Three-dimensional structures of influenza virus neuraminidase-antibody complexes. *Phil. Trans. R. Soc. Lond.* B 323:511–518.

Connolly, M. L. 1983. Solvent-accessible surfaces of proteins and nucleic acids. *Science*. 221:709–713.

Crowther, R. A. 1972. The fast rotation function. *In* The Molecular Replacement Method: A Collection of Papers on the Use of Non-crystallographic Symmetry. M. G. Rossmann, editor. Gordon and Breach, New York. 173–178.

Cruickshank, D. W. J. 1949. The accuracy of electron-density maps in x-ray analysis with special reference to dibenzl. *Acta Crystallogr.* 2:65–82.

Cruickshank, D. W. J. 1950. Corrigenda: the accuracy of electron-density maps in x-ray analysis with special reference to dibenzl. *Acta Crystallogr.* 3:72–73.

Cruickshank, D. W. J. 1954. The accuracy of electron-density maps in x-ray analysis: correction. *Acta Crystallogr.* 7:519.

Cygler, M., and W. F. Anderson. 1988a. Application of the molecular replacement method to multidomain Proteins. 1. Determination of the orientation of an immunoglobulin Fab fragment. *Acta Crystallogr.* A44: 38–45.

Cygler, M., and W. F. Anderson. 1988b. Application of the molecular replacement method to multidomain proteins. 2. Comparison of various methods for positioning an oriented fragment in the unit cell. *Acta Crystallogr.* A44:300–308.

Davies, D. R., E. A. Padlan, and S. Sheriff. 1990. Antibody-antigen complexes. *Annu. Rev. Biochem.* 1990:439–73.

Dombrink-Kurtzman, M. A., L. S. Johnson, G. S. Riordan, W. D. Bedzyk, and E. W. Voss, Jr. 1989. Variable region primary structures of a high affinity anti-fluorescein immunoglobulin M cryoglobulin exhibiting oxazolone cross-reactivity. *J. Biol. Chem.* 264:4513–4522.

Edmundson, A. B., M. Schiffer, K. R. Ely, and M. K. Wood. 1972. Structure of a λ-type Bence-Jones protein at 6-Å resolution. *Biochemistry.* 11:1822–1827.

Eisenberg, D., E. Schwarz, M. Komaromy, and R. Wall. 1984. Analysis of membrane and surface protein sequences with the hydrophobic moment plot. *J. Mol. Biol.* 1984:125–142.

Engh, R. A., and R. Huber. 1991. Accurate bond and angle parameters for x-ray protein structure refinement. *Acta Crystallogr.* A47:392–400.

Fitzgerald, P. M. D. 1988. Merlot, an integrated package of computer programs for the determination of crystal structures by molecular replacement. *J. Appl. Crystallogr.* 21:273–278.

Fujinaga, M., L. T. J. Delbaere, G. D. Brayer, and M. N. G. James. 1985. Refined structure of α-lytic protease at 1.7 Å resolution: analysis of hydrogen bonding and solvent structure. *J. Mol. Biol.* 183:479–502.

Ghiara, J. B., E. A. Stura, R. L. Stanfield, A. T. Profy, and I. A. Wilson. 1994. Crystal structure of the principal neutralization site of HIV-1. *Science*. 264:82–85.

Gibson, A. L., J. N. Herron, X.-M. He, V. A. Patrick, M. L. Mason, J.-N. Lin, D. M. Kranz, E. W. Voss, Jr., and A. B. Edmundson. 1988. Differences in crystal properties and ligand affinities of an antifluorescyl Fab (4–4–20) in two solvent systems. *Proteins*. 3:155–160.

Guy, H. R. 1985. Amino acid side-chain partition energies and distribution of residues in soluble proteins. *Biophys. J.* 47:61–70.

Hendrickson, W. A., and J. H. Konnert. 1981. Stereochemically restrained crystallographic least-squares refinement of macromolecule structures. *In* Biomolecular Structure: Conformation, Function and Evolution. R. Srinivasan, E. Subramanian, and N. Yathindra, editors. Pergamon Press, New York. 43–57.

Herron, J. N. 1984. Equilibrium and kinetic methodology for the measurement of binding properties in monoclonal and polyclonal populations of antifluorescyl-IgG antibodies. *In* Fluorescein Hapten: An Immunological Probe. E. W. Voss, Jr., editor. CRC Press, Boca Raton, Florida. 49–76.

Herron, J. N., X.-M. He, D. W. Ballard, P. R. Blier, P. E. Pace, A. L. M. Bothwell, E. W. Voss, Jr., and A. B. Edmundson. 1991. An autoantibody to single-stranded DNA: comparison of the three-dimensional structures of the unliganded Fab and a deoxynucleotide-Fab complex. *Proteins*. 11:159–175.

Herron, J. N., X.-M. He, M. L. Mason, E. W. Voss, Jr., and A. B. Edmundson. 1989. Three-dimensional structure of a fluorescein-Fab complex crystallized in 2-methyl-2,4-pentanediol. *Proteins*. 5:271–280.

Herron, J. N., D. M. Kranz, D. M. Jameson, and E. W. Voss, Jr. 1986. Thermodynamic properties of ligand binding by monoclonal antifluorescyl antibodies. *Biochemistry*. 25:4602–4609.

Herron, J. N., and E. W. Voss, Jr. 1983. Analysis of heterogeneous dissociation kinetics in polyclonal populations of rabbit anti-fluorescyl-IgG antibodies. *Mol. Immunol.* 20:1323–1332.

Herzberg, O., and J. L. Sussman. 1983. Protein model building by the use of a constrained-restrained least-squares procedure. *J. Appl. Crystallogr.* 16:144–150.

Jacobo-Molina, A., J. Ding, R. G. Nanni, A. D. Clark, Jr., X. Lu, C. Tantillo, R. L. Williams, G. Kamer, A. L. Ferris, P. Clark, A. Hizi,

S. H. Hughes, and E. Arnold. 1993. Crystal structure of human immunodeficiency virus type 1 reverse transcriptase complex with double-stranded DNA at 3.0 Å resolution shows bent DNA. *Proc. Natl. Acad. Sci. USA*. 90:6320–6324.

Kabat, E. A., T. T. Wu, H. M. Perry, K. S. Gottesman, and C. Foeller. 1991. Sequences of Proteins of Immunological Interest, 5th Ed., Vol. 1. National Institutes of Health, Bethesda, MD.

Kellis, J. T., Jr., K. Nyberg, and A. R. Fersht. 1989. Energetics of complementary side-chain packing in a protein hydrophobic core. *Biochemistry*. 28:4914–4922.

Kranz, D. M., J. N. Herron, D. E. Giannis, and E. W. Voss, Jr. 1981. Kinetics and mechanism of deuterium oxide-induced fluorescence enhancement of fluorescyl ligand bound to specific heterogeneous and homogeneous antibodies. *J. Biol. Chem.* 256:4433–4438.

Kranz, D. M., J. N. Herron, and E. W. Voss, Jr. 1982. Mechanisms of ligand binding by monoclonal anti-fluorescyl antibodies. *J. Biol. Chem.* 257: 6987–6995.

Kranz, D. M., and E. W. Voss, Jr. 1981. Partial elucidation of an anti-hapten repertoire in BALB/c mice: comparative characterization of several monoclonal anti-fluorescyl antibodies. *Mol. Immunol.* 18:889–898.

Lattman, E. E., and W. E. Love. 1970. A rotational search procedure for detecting a known molecule in a crystal. *Acta Crystallogr.* B26: 1854–1857.

Luzzati, P. V. 1952. Traitment statistique des erreurs dans la determination des structures cristallines. *Acta Crystallogr.* 5:802–810.

Makhatadze, G. I., and P. L. Privalov. 1990. Heat capacity of proteins I. Partial molar heat capacity of individual amino acid residues in aqueous solution: hydration effect. *J. Mol. Biol.* 213:375–384.

Mian, I. S., A. R. Bradwell, and A. J. Olson. 1991. Structure, function and properties of antibody binding sites. *J. Mol. Biol.* 1991:133–151.

Omelyanenko, V. G., W. Jiskoot, and J. N. Herron. 1993. Role of electrostatic interactions in the binding of fluorescein by anti-fluorescein antibody 4–4–20. *Biochemistry*. 32:10423–10429.

Padlan, E. A., G. H. Cohen, and D. R. Davies. 1985. On the specificity of antibody/antigen interactions: phosphocholine binding to McPC603 and the correlation of three-dimensional structure and sequence data. *Ann. Inst. Pasteur/Immunol.* 136C:271–276.

Padlan, E. A., E. W. Silverton, S. Sheriff, G. H. Cohen, S. J. Smith-Gill, and D. R. Davies. 1989. Structure of an antibody-antigen complex: crystal structure of the HyHel-10 Fab-lysozyme complex. *Proc. Natl. Acad. Sci. USA*. 86:5938–5942.

Prasad, L., S. Sharma, M. Vandonselaar, J. W. Quail, J. S. Lee, E. B. Waygood, K. S. Wilson, Z. Dauter, and L. T. J. Delbaere. 1993. Evaluation of mutagenesis for epitope mapping: structure of an antibody-protein antigen complex. *J. Biol. Chem.* 268:10705–10708.

Privalov, P. L., and G. I. Makhatadze. 1990. Heat capacity of proteins II. Partial molar heat capacity of the unfolded polypeptide chain of proteins: protein unfolding effects. *J. Mol. Biol.* 213:385–391.

Reinitz, D. M., R. Strich, J. F. Scott, and E. W. Voss, Jr. 1988. Anti-fluorescein antibody 3–13 V_H gene rearrangement in idiotypically cross-reactive hybridomas. *Mol. Immunol.* 25:621–630.

Rini, J. M., U. Schulze-Gahmen, and I. A. Wilson. 1992. Structural evidence for induced fit as a mechanism for antibody-antigen recognition. *Science*. 255:959–965.

Rini, J. M., R. L. Stanfield, E. A. Stura, P. A. Salinas, A. T. Profy, and I. A. Wilson. 1993. Crystal structure of a human immunodeficiency virus type 1 neutralizing antibody, 50.1, in complex with its V3 loop peptide antigen. *Proc. Natl. Acad. Sci. USA*. 90:6325–6329.

Rose, G. D., A. R. Geselowitz, G. J. Lesser, R. H. Lee, and M. H. Zehfus. 1985. Hydrophobicity of amino acid residues in globular proteins. *Science*. 229:834–838.

Rossmann, M. G., and D. M. Blow. 1962. The detection of subunits within the crystallographic asymmetric unit. *Acta Crystallogr.* 15:24–32.

Roussel, A., and C. Cambillau. 1989. Turbo-Frodo. *In* Silicon Graphics Geometry Partner Directory. Silicon Graphics, Mountain View, CA. 77–78.

Sharp, K. A., A. Nicholls, R. F. Fine, and B. Honig. 1991. Reconciling the magnitude of the microscopic and macroscopic hydrophobic effects. *Science*. 252:106–109.

Sheriff, S., E. W. Silverton, E. A. Padlan, G. H. Cohen, S. J. Smith-Gill, B. C. Finzel, and D. R. Davies. 1987. Three-dimensional structure of an antibody-antigen complex. *Proc. Natl. Acad. Sci. USA*. 84:8075–8079.

Spolar, R. S., J.-H. Ha, and M. T. Record, Jr. 1989. Hydrophobic effect in protein folding and other noncovalent processes involving proteins. *Proc. Natl. Acad. Sci. USA*. 86:8382–8385.

Stanfield, R. L., T. M. Fieser, R. A. Lerner, and I. A. Wilson. 1990. Crystal structures of an antibody to a peptide and its complex with peptide antigen at 2.8 Å. *Science*. 248:712–719.

Stura, E. A., R. L. Stanfield, T. M. Fieser, R. S. Balderas, L. R. Smith, R. A. Lerner, and I. A. Wilson. 1989. Preliminary crystallographic data and primary sequence for anti-peptide Fab' B13I2 and its complex with the C-helix peptide from myohemerythrin. *J. Biol. Chem.* 264:15721–15725.

Sturtevant, J. M. 1977. Heat capacity and entropy changes in processes involving proteins. *Proc. Natl. Acad. Sci. USA*. 74:2236–2240.

Vix, O., B. Rees, J.-C. Thierry, and D. Altschuh. 1993. Crystallographic analysis of the interaction between cyclosporin A and the Fab Fragment of a monoclonal antibody. *Proteins*. 15:339–348.

Voss, E. W., Jr. 1990. Anti-metatype antibody reactivity: a model for T-cell receptor recognition. *Immunol. Today*. 11:355–357.

Weidner, K. M., and E. W. Voss, Jr. 1991. Immunological characterization of xenogenic anti-metatype antibodies. *J. Biol. Chem.* 266:2513–2519.

Wilson, I. A., J. M. Rini, D. H. Fremont, G. G. Fieser, and E. A. Stura. 1991. X-ray crystallographic analysis of free and antigen-complexed Fab fragments to investigate structural basis of immune recognition. *Methods Enzymol.* 203:153–177.

Wilson, I. A., and R. L. Stanfield. 1993. Antibody-antigen interactions. *Current Opin. Struct. Biol.* 3:113–118.

Wyckoff, H. W., M. Doscher, D. Tsernoglou, T. Inagami, L. N. Johnson, K. D. Hardman, N. M. Allewell, D. M. Kelly, and F. M. Richards. 1967. Design of a diffractometer and flow cell system for x-ray analysis of crystalline proteins with applications to the crystal chemistry of ribonuclease-S. *J. Mol. Biol.* 27:563–578.